Simulation of femtosecond "double-slit" experiments for a chromophore in a dissipative environment

M. F. Gelin, Y. Tanimura, and W. Domcke

Citation: J. Chem. Phys. **139**, 214302 (2013); doi: 10.1063/1.4832876
View online: http://dx.doi.org/10.1063/1.4832876
View Table of Contents: http://jcp.aip.org/resource/1/JCPSA6/v139/i21
Published by the AIP Publishing LLC.

Simulation of femtosecond "double-slit" experiments for a chromophore in a dissipative environment

M. F. Gelin,[1] Y. Tanimura,[1,2] and W. Domcke[1]
[1]*Department of Chemistry, Technische Universität München, Garching D-85747, Germany*
[2]*Department of Chemistry, Graduate School of Science, Kyoto University, Kyoto 606-8502, Japan*

(Received 22 August 2013; accepted 8 November 2013; published online 2 December 2013)

We performed simulations of the prototypical femtosecond "double-slit" experiment with strong pulsed laser fields for a chromophore in solution. The chromophore is modeled as a system with two electronic levels and a single Franck-Condon active underdamped vibrational mode. All other (intra- and inter-molecular) vibrational modes are accounted for as a thermal bath. The system-bath coupling is treated in a computationally accurate manner using the hierarchy equations of motion approach. The double-slit signal is evaluated numerically exactly without invoking perturbation theory in the matter-field interaction. We show that the strong-pulse double-slit signal consists of a superposition of N-wave-mixing (N = 2, 4, 6...) responses and can be split into population and coherence contributions. The former reveals the dynamics of vibrational wave packets in the ground state and the excited electronic state of the chromophore, while the latter contains information on the dephasing of electronic coherences of the chromophore density matrix. We studied the influence of heat baths with different coupling strengths and memories on the double-slit signal. Our results show that the double-slit experiment performed with strong (nonperturbative) pulses yields substantially more information on the photoinduced dynamics of the chromophore than the weak-pulse experiment, in particular, if the bath-induced dephasings are fast. © *2013 AIP Publishing LLC*. [http://dx.doi.org/10.1063/1.4832876]

I. INTRODUCTION

In 1991, Scherer and co-workers[1,2] reported on a pioneering femtosecond "double-slit" experiment in the gas phase. They used two phase-locked pump pulses to excite molecular iodine into its *B* state and measured the total fluorescence from this state as a function of the time delay between the two pulses. Although the signal yields the total electronic population of the *B* state and, as such, is incoherent, the information about the evolution of electronic coherences of the iodine density matrix is imprinted into it through the relative phase of the pulses. Similar experiments were later performed for alkali atoms (see the reviews [3–5]) and for molecular species, both in the gas phase[6,7] and in the condensed phase.[8] These experiments can be viewed as realizations of Ramsey-type spectroscopy [9–11] or wave-packet interferometry.[3–5]

The double-slit experiment of Scherer *et al.*[1,2] was performed with weak pulses. The measured signal is, therefore, related to the linear response function of the material system. Despite the apparent advantage of the detection of interferograms as oscillatory transients in the time domain, the information content of this experiment is similar to that provided by linear absorption spectroscopy.[12–14]

Subsequent generalizations of the double-slit experiment have been developed along two major directions. The first employs multiple phase-locked pulses and constitutes the field of multi-pulse wave-packet interferometry.[3–5] The second direction, double-slit interferometry with strong laser pulses, is the focus of the present paper. A "strong" pulse is defined here as a laser pulse which causes a significant depopulation (population) of the initial (final) electronic state. The strength criterion thus depends not only on the laser intensity but also on the oscillator strength of the transition and the detuning of the carrier frequency from the electronic transition.

It was shown theoretically and demonstrated experimentally for electron wave packets in atoms that strong-field double-slit signals not only exhibit high-frequency oscillatory responses corresponding to transitions between the ground state and two excited states (three-level system) but also exhibit a slower beating with the frequency corresponding to the energy difference between the two excited states.[14–16] The latter beating is absent in linear response and is, therefore, a characteristic feature of the strong-field regime.

The reviews[3,17] summarize recent progress in strong-pulse interferometry and control. The strong-field double-slit phenomenon is also the key to femtosecond single-molecule spectroscopy[18,19] and control.[20] In Refs. 21 and 22 it was shown that a whole series of nonlinear N-wave-mixing (4WM, 6WM, ...) measurements can be performed with a single double-pulse setup, using the pulse strength for the amplification of 6WM and higher-order contributions to the measured signal. Experiments with strong phase-locked pulses may yield more information on the dynamics of the material system than traditional linear or weak-pulse 4WM spectroscopies. On the other hand, the complexity of the responses induced by multiple strong laser pulses makes the interpretation of the signals difficult and requires theoretical support.

In the present work, a comprehensive theoretical study of the prototypical double-slit experiment has been performed, considering a model of a photochemically nonreactive chromophore in a dissipative environment. In the simulations of

the double-slit signal we have avoided several commonly used approximations, notably the assumption of weak laser-matter interaction, the weak system-bath coupling approximation, and the Markovian approximation. Starting from generic system-bath and system-field interaction Hamiltonians, the signals are computed numerically accurately using the hierarchy equation of motion (HEOM) method.[23–26] We have systematically studied how heat baths with different coupling strengths and memories affect the signal.

The outline of the article is as follows. We start by introducing the appropriate Hamiltonian (Sec. II) and providing the theoretical expression for the double-slit signal (Sec. III). In Secs. IV and V, we discuss two approximate methods of the calculation of the signal, which are based on the perturbative treatment of the system-field interaction (Sec. IV) and the strong-pulse doorway-window (DW) picture (Sec. V). In Secs. IV and V we develop a qualitative description of the double-slit signal. The actual calculations are performed with the HEOM method as detailed in Sec. VI. The results of these calculations are reported and discussed in Sec. VII. The conclusions are given in Sec. VIII.

II. THE HAMILTONIAN

We consider a chromophore immersed in a solvent. In the strong-pulse double-slit experiment, two resonant phase-locked pulses induce multiple transitions between the electronic ground state, g, and the lowest bright excited electronic state, e, of the chromophore. For simplicity and clarity, the latter is assumed to possess a single harmonic Franck-Condon (FC) active vibrational mode, which is included in the primary system. All other vibrational modes of the chromophore and the solvent are treated as a harmonic heat bath. The total Hamiltonian of the material system is thus expressed as[27]

$$\hat{H}_M \equiv \hat{H}_{FC} + \hat{H}_B + \hat{H}_{SB}, \tag{2.1}$$

where

$$\hat{H}_{FC} = \sum_{k=g,e} |k\rangle \left(\frac{1}{2}\hbar\Omega[P^2 + (Q - \Delta_k)^2] + \varepsilon_k \right) \langle k| \tag{2.2}$$

and

$$\hat{H}_B + \hat{H}_{SB} = \sum_{\alpha} \sum_{k=g,e} |k\rangle \left(\frac{1}{2}\hbar\omega_\alpha \left[p_\alpha^2 + \left(q_\alpha - \Delta_k^\alpha \right)^2 \right] \right) \langle k|. \tag{2.3}$$

Here, the bra-ket notation is used to denote the electronic states. Q, P, and Ω are the dimensionless normal coordinate, momentum, and frequency of the FC mode, whereas q_α, p_α, and ω_α are the coordinate, momentum, and frequency of the αth bath mode. The dimensionless displacement of the FC mode is denoted by Δ_e, while the displacement of the αth bath mode is denoted as Δ_k^α (for simplicity, we set $\Delta_g = 0$ and $\Delta_g^\alpha = -\Delta_e^\alpha$). ε_e is the vertical electronic excitation energy ($\varepsilon_g = 0$).

In the present work, we are interested in the dynamics of the primary system on the timescale of several vibrational periods $2\pi/\Omega$ of the system mode. The bath gives rise to pure electronic dephasing due to the modulation of the energy gap between the electronic ground state and the excited state of the chromophore. To describe the bath-induced dephasing, it is convenient to incorporate the energies $\sum_\alpha \hbar\omega_\alpha(\Delta_e^\alpha)^2/2$ into ε_e and rewrite the bath Hamiltonian as

$$\hat{H}_B + \hat{H}_{SB} = \sum_\alpha \left\{ \frac{1}{2}\hbar\omega_\alpha \left(p_\alpha^2 + q_\alpha^2 \right) + c_\alpha q_\alpha \hat{V} \right\}, \tag{2.4}$$

where $\hat{V} = |e\rangle\langle e| - |g\rangle\langle g|$ and $c_\alpha = -\omega_\alpha \Delta_e^\alpha$. The influence of the bath on the system dynamics is fully determined by its spectral density

$$J(\omega) = \sum_\alpha \frac{c_\alpha^2}{2m_\alpha\omega_\alpha}\delta(\omega - \omega_\alpha). \tag{2.5}$$

The Hamiltonian specified by Eqs. (2.1)–(2.5) does not include a direct coupling of the system mode Q with the bath modes q_k, since our intention is to model an underdamped bath mode. A bilinear coupling of the system mode with the bath modes could be included in the Hamiltonian if this should be necessary for the simulation of a specific experiment.

The interaction of the chromophore with the laser pulses can be written in the rotating-wave approximation (RWA) and in the Condon approximation as follows (see Ref. 28 for a discussion of the validity of the RWA for moderately strong pulses):

$$\hat{H}_F(t) = -\lambda_p X^\dagger (E(t)e^{i(\phi_1 - \omega_p t)} + E(t-\tau)e^{i(\phi_2 - \omega_p(t-\tau))}) + H.c. \tag{2.6}$$

Here,

$$X = |g\rangle\langle e|, \;\; X^\dagger = |e\rangle\langle g| \tag{2.7}$$

is the electronic transition operator, λ_p is given by the dot product of the laser field amplitude and the transition dipole moment, ω_p is the carrier frequency of the pulses, ϕ_1 and ϕ_2 are their phases, and $E(t)$ is the pulse envelope.

The total (chromophore + solvent) dynamics driven by the laser field is described by the Liouville–von Neumann equation,

$$\frac{\partial}{\partial t}\hat{\rho}_{tot}(t) = -\frac{i}{\hbar}\hat{H}_{tot}^\times(t)\hat{\rho}_{tot}, \tag{2.8}$$

where

$$\hat{H}_{tot}(t) = \hat{H}_M + \hat{H}_F(t) \tag{2.9}$$

is the total Hamiltonian and

$$\hat{A}^\times\hat{\rho} = \hat{A}\hat{\rho} - \hat{\rho}\hat{A}$$

for any operator $\hat{A}$. The reduced density matrix, defined as

$$\hat{\rho}(t) \equiv \mathrm{Tr}_B\{\hat{\rho}_{tot}(t)\} = \sum_{k,n=g,e} |k\rangle\rho_{kn}(t)\langle n|, \tag{2.10}$$

is the key object for the evaluation of the signal. The HEOM method permits the exact evaluation of $\hat{\rho}(t)$ (see Sec. VI).

The chromophore + solvent Hamiltonian defined by Eqs. (2.1), (2.2), and (2.4) can be regarded as a generalized spin-boson Hamiltonian, that is, all vibrational modes couple linearly with the electronic system. A bilinear coupling of the system mode with the bath modes, which would lead to energy relaxation of the system mode, is not considered here,

but could be taken into account within the Brownian oscillator model[27] and treated with the HEOM method.[29–31] Using the bath Hamiltonian (2.4), we can study bath-induced pure dephasing of the density matrix, which is not "contaminated" by vibrational energy relaxation of the system mode.

III. DOUBLE-SLIT SIGNAL AND NONLINEAR POLARIZATION

As observable, we consider the integral fluorescence from the excited electronic state, e, as a function of τ, the time delay between the two pump pulses. This signal is proportional to the population of the excited electronic state after the interaction with both laser pulses:

$$S(\tau) = \langle |e\rangle\langle e|\hat{\rho}(t \to \infty)\rangle\,, \tag{3.1}$$

where the reduced density matrix $\hat{\rho}(t)$ is defined by Eq. (2.10) and angular brackets indicate the trace over the degrees of freedom of the primary system.

The signal can alternatively be expressed through the total complex nonlinear polarization

$$P(t) = \langle X^{\dagger}\hat{\rho}(t)\rangle \tag{3.2}$$

as follows:

$$S(\tau) = -2\mathrm{Im}\int_{-\infty}^{\infty} dt\, E(t-\tau)e^{i(\phi_2 - i\omega(t-\tau))}P(t). \tag{3.3}$$

(See Refs. 1 and 12.) Equation (3.3) can be derived by the multiplication of both sides of Eq. (2.8) by $|e\rangle\langle e|$, formal integration over time from $-\infty$ to ∞, and taking the trace. Equation (3.3) is reminiscent of the formula for the intensity of the integral transient absorption pump-probe signal,[27] but differs from it in two respects. (i) $P(t)$ is the total, rather than the phase-matched, polarization, and (ii) $P(t)$ is the nonlinear polarization which contains all possible contributions in the system-field interaction. As we will see, these two facts have interesting consequences.

Since we are interested in the short-time behavior of the signal (on a timescale of several vibrational periods of the FC-active mode), we can safely neglect the reorientation dynamics of the chromophore. To perform the ensemble average over the orientation of the chromophore, λ_p should be replaced by $\lambda_p \cos(\vartheta)$ in Eq. (2.6), where ϑ is the angle between the direction of the polarization vector of the pump pulses and the transition dipole moment. This renders the signal explicitly ϑ-dependent, $S(\tau, \lambda_p \cos(\vartheta))$. The ensemble-averaged signal is then given by the expression[32]

$$\bar{S}(\tau) = {}^1\!/_2 \int_{-1}^{1} dx\, S(\tau, \lambda_p x), \tag{3.4}$$

where $x \equiv \cos(\vartheta)$. According to the mean-value theorem, the integral in Eq. (3.4) can be formally evaluated as

$$\bar{S}(\tau) = S(\tau, \lambda_p \bar{x}), \tag{3.5}$$

where $-1 \le \bar{x} \le 1$ is a certain (unknown) value of x. Thus, ensemble averaging over molecular orientations is equivalent to a renormalization of the pulse strength, $\lambda_p \to \lambda_p \bar{x}$. Since the value of $\bar{x}$ is unknown, orientational averaging is a nuisance for coherent control studies (see, e.g., Refs. 18 and 33), but is not a severe problem for the simulation and interpretation of double-slit experiments.

IV. PERTURBATIVE DESCRIPTION

It is insightful to consider the expansion of the signal in powers of the pulse strength λ_p,

$$S(\tau) = \sum_{n=1}^{\infty} \lambda_p^{2n} S_n(\tau). \tag{4.1}$$

In principle, the total Hamiltonian $\hat{H}_{tot}(t)$, defined as the sum of the Hamiltonians (2.2), (2.4), and (2.6), permits the evaluation of any $S_n(\tau)$.[34,35] However, the expressions for higher-order contributions are rapidly becoming cumbersome. In the leading order, we have

$$S_1(\tau) = \sigma_1(\tau) + \sigma_1(-\tau) + 2\sigma_1(0), \tag{4.2}$$

where

$$\sigma_1(\tau) = -2\mathrm{Re}\int_{-\infty}^{\infty} dt \int_0^{\infty} dt_1 E(t-\tau)E^*(t-t_1)e^{i(\omega_p\tau + \Delta\phi)} \times e^{-i(\omega_p - \varepsilon_e/\hbar - \Omega\Delta_e^2/2)t_1 - g(t_1)}, \tag{4.3}$$

$\Delta\phi \equiv \phi_2 - \phi_1$, and $g(t) \equiv g(-t)$ is the lineshape function.[27] For the Drude spectral density (see Sec. VI below), $g(t)$ can be evaluated analytically (see Appendix A). For delta-function pulses with $\Delta\phi = 0$, Eq. (4.3) yields

$$S(\tau) \sim \mathrm{Re}\, e^{-i(\varepsilon_e/\hbar + \Omega\Delta_e^2/2)\tau - g(\tau)} + \mathrm{const}, \tag{4.4}$$

which reveals that $S(\tau)$ oscillates with the frequency $\approx \varepsilon_e/\hbar \approx \omega_p$.

In the frequency domain, Eq. (4.3) yields

$$\int_{-\infty}^{\infty} d\tau e^{i\omega\tau}[S_1(\tau) - 2\sigma_1(0)] = -2|E(\omega)|^2 I(\omega), \tag{4.5}$$

where

$$I(\omega) = \mathrm{Re}\int_0^{\infty} d\tau e^{i(\omega - \varepsilon_e/\hbar - \Omega\Delta_e^2/2)\tau - g(\tau)} \tag{4.6}$$

is the linear absorption spectrum. For weak pulses (i.e., in the leading (linear) order in λ_p), the Fourier transform of $S(\tau)$ yields, therefore, the linear absorption spectrum multiplied by the spectral intensity of the pulses (cf. Refs. 1, 2, and 12).

While it is possible to explicitly write down higher-order contributions to Eq. (4.1) (see, e.g, Ref. 36 for the third-order description of the experiment of Ref. 1), the expressions are cumbersome and knowing them explicitly is of little value for the present discussion. Note that $S_2(\tau)$, for example, contains not only the terms contributing to the corresponding third-order pump-probe signal (i.e., terms quadratic in the amplitudes of the pulses #1 and #2) but also terms which are, for example, linear in the amplitude of pulse #1 and cubic in the amplitude of pulse #2. In general, the n-order terms consist of a time-independent background and a time-dependent response. The existence of a field-dependent background is common for strong-pulse signals (see, e.g., Refs. 16 and 37).

Experimentally, one can get rid of the background signal by applying phase cycling (cf. Refs. 21 and 22).

V. DOORWAY-WINDOW PICTURE

The doorway (D)–window (W) representation of optical third-order spectroscopy has been introduced by Yan, Fried, and Mukamel.[27,38,39] It was further developed towards pulses of arbitrary strength in Ref. 40. If the two pump pulses are temporally well separated, the double-slit signal could, in principle, be calculated within the strong-pulse DW approximation. While the DW approximation becomes exact for non-overlapping pulses and the isolated chromophore, this is not necessarily true for the chromophore in solution due to the finite memory induced by the coupling of the chromophore to the bath. Since the validity of the DW approximation is not guaranteed for non-Markovian open systems,[32,41] we did not use it in the actual calculations. The DW approximation is useful, however, for the qualitative interpretation of the signals computed with the HEOM method.

As is explained in Appendix B, the strong-pulse double-slit signal consists of population and coherence contributions,

$$S(\tau) = S^{(p)}(\tau) + S^{(c)}(\tau). \tag{5.1}$$

The population part $S^{(p)}(\tau)$ reflects the dynamics of vibrational wave packets in the g and e states,

$$S^{(p)}(\tau) = \mathrm{Im}\left\langle W_{gg}G_{gg}(\tau)D_{gg} + W_{ee}G_{ee}(\tau)D_{ee}\right\rangle. \tag{5.2}$$

Here and below $G_{kn}(\tau) \equiv \langle k|G(\tau)|n\rangle$, $k, n = g, e$, is the field-free evolution operator of the primary system. D_{kk} is the doorway operator (generating the wave packet prepared by the pulse #1) and W_{kk} is the window operator (generating the wave packet prepared by the pulse #2), see Appendix B for details. $S^{(c)}(\tau)$ describes the time evolution of the coherence between the g and e states:

$$S^{(c)}(\tau) = \mathrm{Im}\left\langle W_{ge}G_{eg}(\tau)D_{eg}e^{i\omega_p\tau} + W_{eg}G_{ge}(\tau)D_{ge}e^{-i\omega_p\tau}\right\rangle. \tag{5.3}$$

Equations (5.1)–(5.3) emphasize the double-slit character of the signal. Indeed, $S^{(p)}(\tau)$ represents the sum of the intensities arising from the g and e states. This contribution yields the strong-pump strong-probe signal considered in Refs. 40 and 42 and does not require phase-locked pulses. In the present case, it exhibits beatings due to vibrational wave-packet motion of the underdamped FC-active mode. The coherent part $S^{(c)}(\tau)$ describes the interference of the signals arising from the g and e states. It reflects the evolution of electronic coherences and vanishes when the two pump pulses are not phase-locked. $S^{(c)}(\tau)$ exhibits fast oscillations with the optical frequency ω_p, depends on the phase difference $\Delta\phi$ between the pulses (see Eqs. (B4) and (B5)), and is sensitive to the bath-induced dephasing.

VI. SIMULATION OF THE SIGNAL WITH THE HEOM METHOD

The dynamics of the primary system and the double-slit signal (Eq. (3.1)) are described by the reduced density matrix $\hat\rho(t)$ (Eq. (2.10)), which is obtained from the total density matrix by tracing out the bath degrees of freedom. In the present work, we employed the Drude spectral distribution for the bath oscillators,

$$J(\omega) = \frac{\lambda_2}{\pi}\frac{\gamma\omega}{\gamma^2+\omega^2}. \tag{6.1}$$

Here, λ_2 determines the strength of the system-bath coupling and γ is a measure of the width of the spectral density distribution. For this bath, $\hat\rho(t)$ can be evaluated with the HEOM method, which takes account of non-Markovian effects and nonperturbative system-bath interactions at finite temperature numerically accurately.[23–26] The HEOM method has been used to study linear and nonlinear spectroscopy,[43–46] quantum information,[47–49] exciton transfer,[50–54] and electron transfer.[29–31,55] For the present application, it is crucial that the interaction of the system with a time-dependent external field can be added while taking the system-bath quantum entanglement into account through the hierarchy elements.[56]

The symmetric and antisymmetric bath correlation functions for the Drude spectral density (6.1) are given in Appendix A, see Eqs. (A11) and (A12). For the application of the HEOM method to the present problem, we approximate the symmetric bath correlation function with negligible error at the desired temperature $1/\beta\hbar$ as

$$C_2(t) \approx \lambda_2\gamma\left\{\frac{1}{2}\cot\left(\frac{\beta\hbar\gamma}{2}\right)\mathrm{e}^{-\gamma t} + \frac{2}{\beta\hbar}\sum_{k=1}^{K}\frac{\nu_k}{\nu_k^2-\gamma^2}\mathrm{e}^{-\nu_k t}\right\} + \lambda_2\left(\frac{1}{\gamma\beta\hbar} - \cot\left(\frac{\beta\hbar\gamma}{2}\right) - \frac{2\gamma}{\beta\hbar}\sum_{k=1}^{K}\frac{1}{\nu_k^2-\gamma^2}\right)\delta(t). \tag{6.2}$$

This approximation is equivalent to assuming that the Matsubara times, ν_k^{-1}, are shorter than all relevant system times for $k > K$, so that $\nu_k\exp(-\nu_k t) \approx \delta(t)$. K is the cutoff of the sum over the Matsubara frequencies in Eq. (6.2).

According to Refs. 23–26, the HEOM method is formulated as follows. We denote the number of the hierarchy elements corresponding to $\exp(-\gamma t)$ in Eq. (6.2) as n and the number of the hierarchy elements corresponding to the kth Matsubara exponential $\exp(-\nu_k t)$ in Eq. (6.2) as j_k. The HEOM equations are then written as

$$\begin{aligned}\frac{\partial\hat\rho^{(n)}_{j_1\cdots j_K}(t)}{\partial t} = &-\left[\frac{i}{\hbar}\hat H^{\times}(t) + n\gamma + \sum_{k=1}^{K}j_k\nu_k + \hat\Xi\right]\hat\rho^{(n)}_{j_1\cdots j_K}(t)\\ &+ \hat V^{\times}\hat\rho^{(n+1)}_{j_1\cdots j_K}(t) + n\hat\Theta\hat\rho^{(n-1)}_{j_1\cdots j_K}(t)\\ &+ \sum_{k=1}^{K}\hat V^{\times}\hat\rho^{(n)}_{j_1\cdots,j_k+1,\cdots j_K}(t)\\ &+ \sum_{k=1}^{K}j_k\nu_k\hat\Psi_k\hat\rho^{(n)}_{j_1\cdots,j_k-1,\cdots j_K}(t).\end{aligned} \tag{6.3}$$

In these equations,

$$\hat H(t) = \hat H_{FC} + \hat H_F(t) \tag{6.4}$$

is the Hamiltonian of the driven primary system,

$$\hat{\Theta} = \frac{i\lambda_2\gamma}{2}\left[-i\hat{V}^{\circ} + \cot\left(\frac{\beta\hbar\gamma}{2}\right)\hat{V}^{\times}\right], \tag{6.5}$$

$$\hat{\Psi}_k = i\frac{2\lambda_2\gamma}{\beta\hbar}\frac{\nu_k}{\nu_k^2 - \gamma^2}\hat{V}^{\times}, \tag{6.6}$$

$\hat{A}^{\circ}\hat{\rho} = \hat{A}\hat{\rho} + \hat{\rho}\hat{A}$ for any operator $\hat{A}$ and $\hat{\Xi} = -i\hat{V}^{\times}\sum_{k=K+1}^{\infty}\hat{\Psi}_k$. The HEOM consists of an infinite number of equations, but they can be truncated at finite order with negligible error.[23–26] Essentially, the condition necessary for the error introduced by the truncation to be negligibly small is that the total number of hierarchy elements or the total number of Matsubara frequencies retained be sufficiently large. Explicitly, it can be shown that the condition $n\gamma + \sum_{k=1}^{K} j_k\nu_k \gg \max\{\Omega, \lambda_p\}$, where Ω is the oscillator frequency of the FC-active mode (Eq. (2.2)) and λ_p is the amplitude of the system-field interaction (Eq. (2.6)), is sufficient for this purpose. Then the infinite hierarchy of Eq. (6.3) can be truncated by the terminator for the deeper hierarchy $\hat{\rho}^{(n+1)}_{j_1\cdots j_K}(t)$ and $\hat{\rho}^{(n)}_{j_1\cdots,\, j_k+1,\cdots j_K}(t)$ as

$$\frac{\partial\hat{\rho}^{(n)}_{j_1\cdots j_K}(t)}{\partial t} \approx -\left[\frac{i}{\hbar}\hat{H}^{\times}(t) + n\gamma + \sum_{k=1}^{K} j_k\nu_k + \hat{\Xi}\right]\hat{\rho}^{(n)}_{j_1\cdots j_K}(t). \tag{6.7}$$

The inclusion of an underdamped Brownian oscillator mode instead of a Drude mode is also possible,[29–31,56] but the calculations become computationally more demanding. In such cases, a variety of techniques have been developed to accelerate the numerical performance of the HEOM method.[57–62] It should be noted that the HEOM scheme breaks down when the heat bath is at zero temperature ($\beta = \infty$), since the factors in Eq. (6.3) diverge.

The 0th element of the hierarchy is identical to the reduced density operator $\hat{\rho}(t) = \hat{\rho}^{(0)}_{0,\cdots 0}(t)$ defined in Eq. (2.10). The higher-order elements $\hat{\rho}^{(n)}_{j_1\cdots j_K}(t)$ are introduced to account for nonperturbative and non-Markovian system-bath interactions. Although these elements do not have a direct physical meaning, they allow us to take into account the quantum entanglement between the system and the bath.[47–49]

We use dimensionless variables throughout this article, measuring frequencies in units of a certain frequency $\Omega_0 = 1$, and time in units of Ω_0^{-1}. We take the frequency of the FC-active mode as $\Omega = 3$, so that the vibrational period is $\tau_\Omega = 2\pi/3 \approx 2.1$. The dimensionless horizontal shift of the potential curves of the FC mode is taken as $\Delta_e = 1$. The carrier frequencies of the pulses are the same, $\omega_p = 47$, and the optical period $\tau_{op} = 2\pi/\omega_p \approx 0.13$. The pulse envelopes are Gaussian,

$$E(t) = \exp\left\{-4\ln 2\left(\frac{t}{\tau_p}\right)^2\right\}, \tag{6.8}$$

where τ_p is the pulse duration (full width at half maximum of the amplitude). In the simulations, we assume that the pulses possess the same waveform, so that their phase shift is $\Delta\phi \equiv \phi_2 - \phi_1 = 0$. This choice renders the pulses #1 and #2 equivalent and hence $S(\tau) = S(-\tau)$. In what follows, we show $S(\tau)$ for $\tau \geq 0$. We assume resonant excitation, $\omega_p = \varepsilon_e + \Omega$. A slight detuning of ω_p (of the order of the vibrational frequency Ω) does not qualitatively alter the results.

The dynamics of the FC mode is described by six vibrational basis functions in each (ground and excited) electronic state. The inclusion of additional vibrational basis functions does not change the results. The spectral width γ of the bath, the system-bath coupling λ_2, the temperature parameter $\beta\hbar\Omega_0$, as well as the pulse strength λ_p and the pulse duration τ_p are varied. The numerical integration of the HEOM equations is performed with the 4th-order Runge-Kutta method. The hierarchy equations are truncated at $N = 12$ and $K = 3$.

VII. DOUBLE-SLIT SIGNALS

The problem under study involves several timescales. The fastest is the optical period $\tau_{op} = 2\pi/\omega_p$. The next is the vibrational period $\tau_\Omega = 2\pi/3$ of the FC-active mode, which, in our calculations, is 15.7 times longer than τ_{op}. The third characteristic time is the pulse duration τ_p and the fourth is a characteristic dephasing time.

Figure 1 shows $S(\tau)$ in the simplest case of bath-free evolution. Panels (a) and (b) correspond to weak ($\lambda_p = 0.01$) and

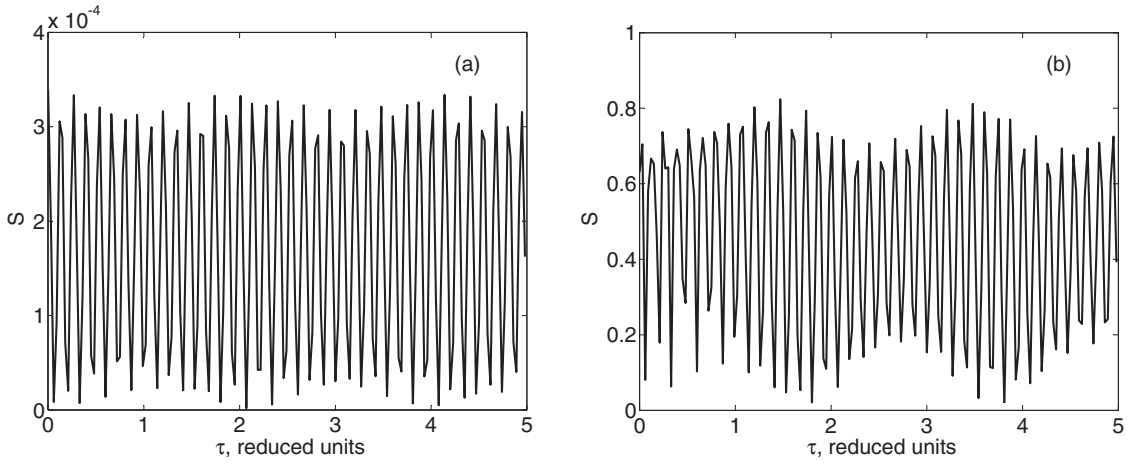

FIG. 1. Double-slit signal $S(\tau)$ for the isolated chromophore and weak (panel (a), $\lambda_p = 0.01$) and strong (panel (b), $\lambda_p = 1$) as well as short ($\tau_p = 1.2$) pulses at ambient temperature ($\beta\hbar\Omega_0 = 0.5$).

strong ($\lambda_p = 1$) pulses, respectively. The signals in both panels oscillate with the pulse carrier frequency ω_p (fast beatings), superimposed on which are slower beatings with the vibrational frequency Ω. Weak pulses promote only a small fraction of the initial ground-state population to the excited electronic state, while strong pulses may depopulate the ground state significantly. In any case, the information content of the double-slit experiment on the isolated chromophore is independent of the pulse strength.

The situation changes if the system is not isolated from its environment. Figure 2 shows signals for excitation by weak pulses ($\lambda_p = 0.01$). The system-bath coupling is moderate

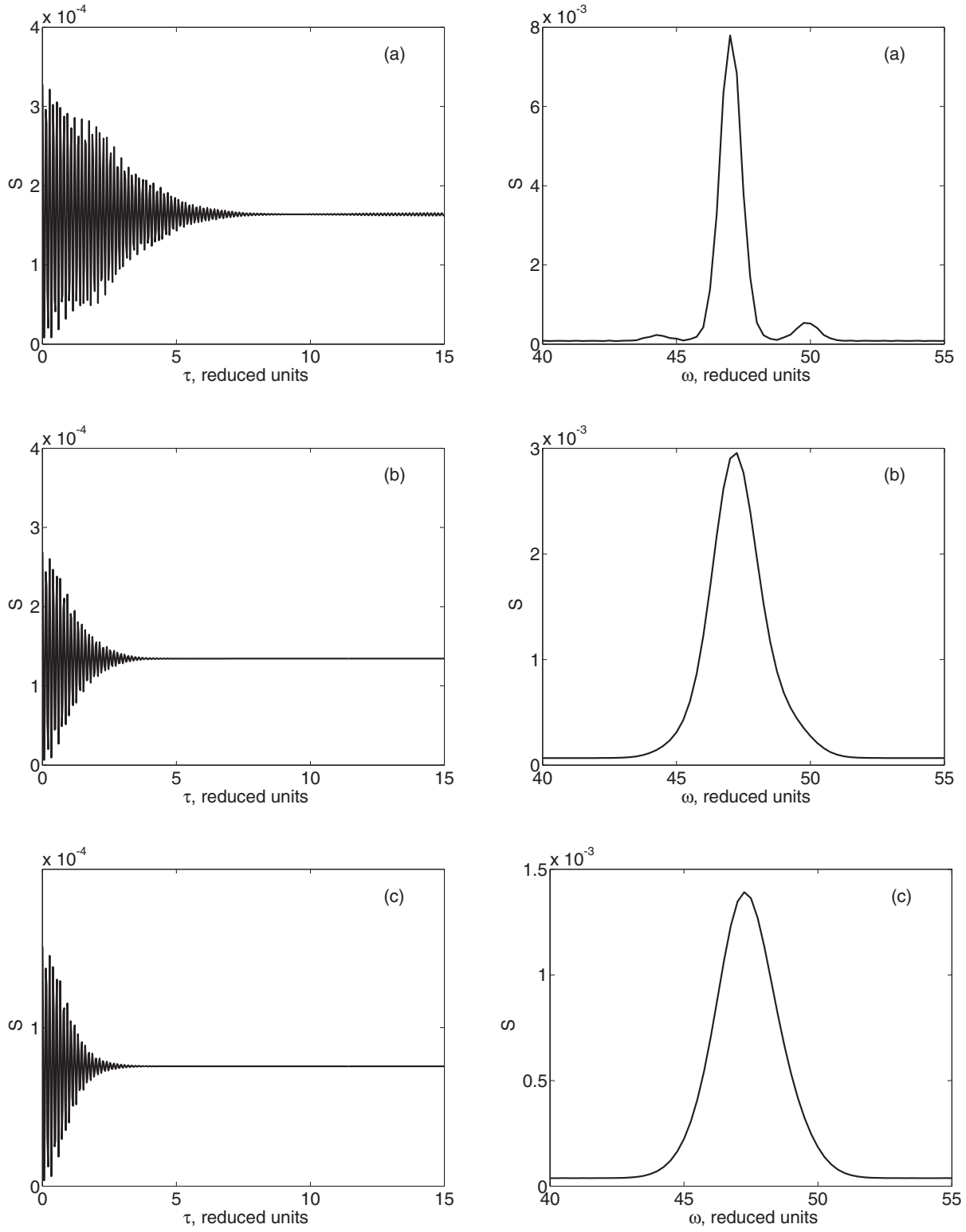

FIG. 2. Double-slit signal, $S(\tau)$, (left column) and real part of its Fourier transform, $S(\omega)$, (right column). The chromophore is excited by weak ($\lambda_p = 0.01$) and short ($\tau_p = 1.2$) pulses. The system-bath coupling is moderate ($\lambda_2 = 1$). The width of the spectral function of the bath is $\gamma = 0.1$ (panel (a)), $\gamma = 1$ (panel (b)), $\gamma = 10$ (panel (c)). The temperature is ambient ($\beta\hbar\Omega_0 = 0.5$).

($\lambda_2 = 1$). It has been chosen such that it cannot be ignored on the timescale of the experiment. The left column shows the double-slit signal $S(\tau)$, while the right column shows its Fourier transform, $S(\omega)$. The panels (a) through (c) correspond to different width parameters γ of the spectral density of Eq. (6.1). The temperature is chosen as $\beta\hbar\Omega_0 = 0.5$ (ambient temperature).

We first consider $S(\tau)$ in the time domain (left panels). In panel (a), $\gamma = 0.1$, which corresponds to inhomogeneous broadening ($\exp(-g_2(t))$ of Eq. (A13) is approximately Gaussian). In panel (c), $\gamma = 10$, which represents the limit of the homogeneous broadening ($\exp(-g_2(t))$ of Eq. (A13) is approximately exponential). Panel (b) represents an intermediate situation ($\gamma = 1$). Since $\exp(-\gamma t)$ can be interpreted as the memory function of the bath, the bath of panel (a) ($\gamma = 0.1$) can be regarded as highly non-Markovian, while the bath of panel (c) ($\gamma = 10$) is almost Markovian. For fixed system-bath coupling strength λ_2, the decay of the signal

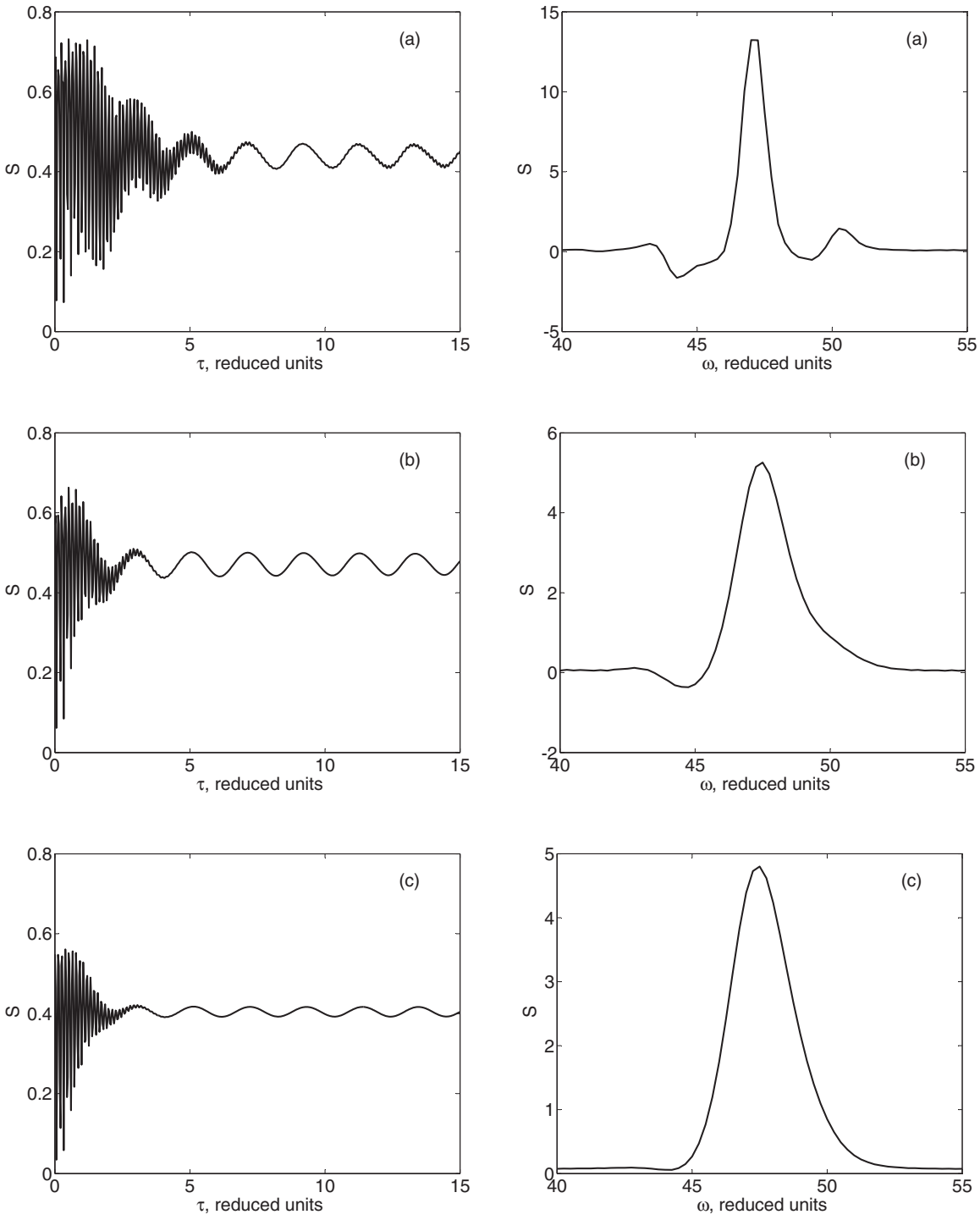

FIG. 3. Double-slit signal, $S(\tau)$, (left column) and real part of its Fourier transform, $S(\omega)$, (right column). The chromophore is excited by strong ($\lambda_p = 1$) and short ($\tau_p = 1.2$) pulses. The system-bath coupling is moderate ($\lambda_2 = 1$). The width of the spectral function of the bath is $\gamma = 0.1$ (panel (a)), $\gamma = 1$ (panel (b)), $\gamma = 10$ (panel (c)). The temperature is ambient ($\beta\hbar\Omega_0 = 0.5$).

accelerates from panel (a) to panel (c). In all three cases, the system-bath coupling is moderate, in the sense that the signals decay on timescales which are longer than τ_Ω. Note that the signals of Fig. 2 exhibit no indication of the chromophore vibration.

Consider next the Fourier-transformed spectra $S(\omega)$ in the right column of Fig. 2. The weak-pulse double-slit signal as well as the linear absorption spectrum $I(\omega)$ (Eq. (4.6)) are determined by the linear (in λ_p) contribution to the polarization. The signal $S(\omega)$ in panel (a) corresponds to a narrow spectral density of the bath and exhibits a certain vibrational structure. If the spectral density becomes broader (panels (b) and (c)), $S(\omega)$ exhibits only a single broad peak. Due to the finite spectral width of the pulses (the factor $|E(\omega)|^2$ in Eq. (4.5)), the weak-pulse double-slit signal $S(\tau)$ reproduces $I(\omega)$ only within the frequency window of the pump pulses. The weak-pulse double-slit signal, therefore, contains less information than $I(\omega)$.

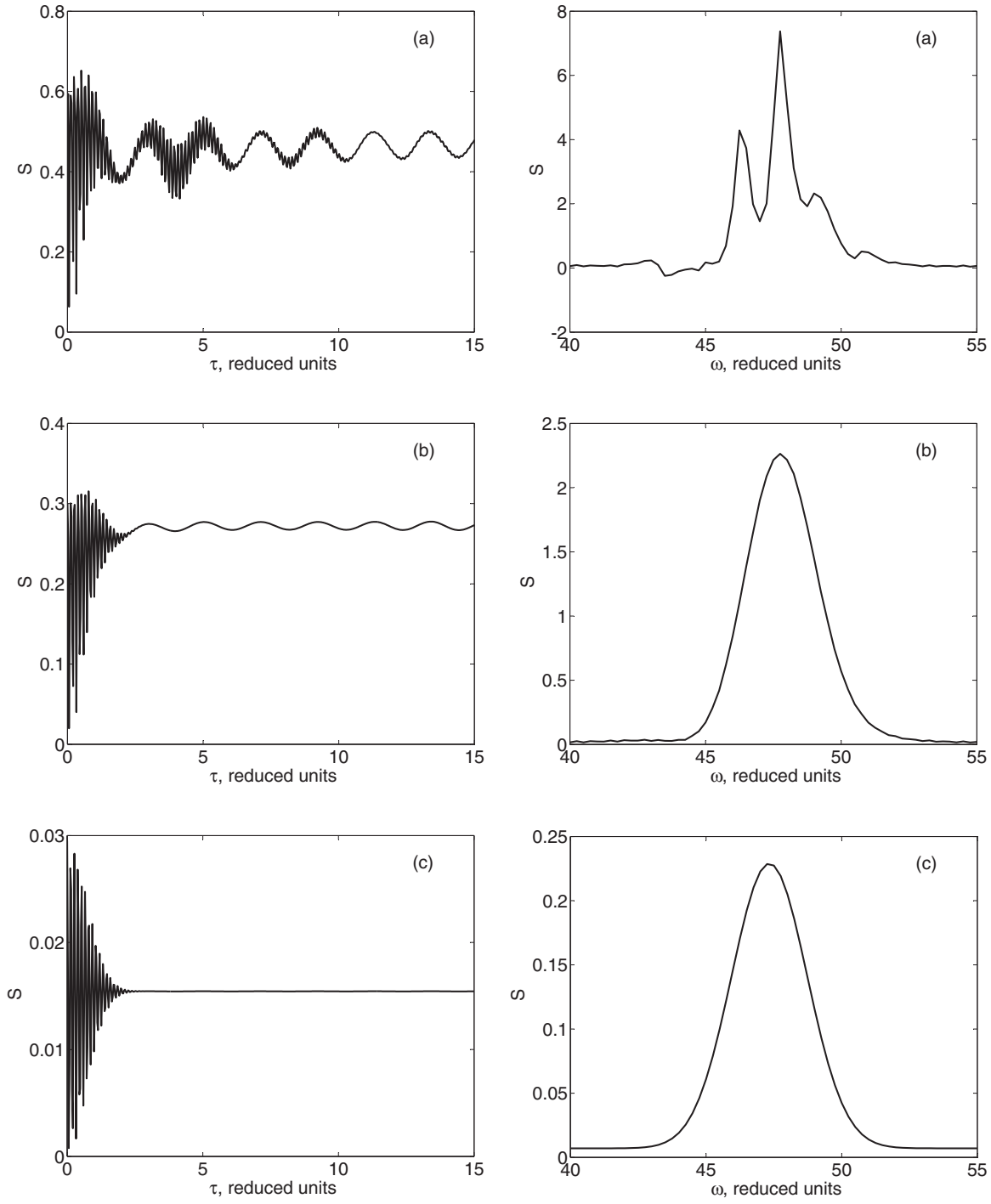

FIG. 4. Double-slit signal, $S(\tau)$, (left column) and real part of its Fourier transform, $S(\omega)$, (right column). The chromophore is excited by strong ($\lambda_p = 1$) and short ($\tau_p = 1.2$) pulses. The system-bath coupling is strong ($\lambda_2 = 10$). The width of the spectral function of the bath is $\gamma = 0.1$ (panel (a)), $\gamma = 1$ (panel (b)), $\gamma = 10$ (panel (c)). The temperature is ambient ($\beta\hbar\Omega_0 = 0.5$).

The situation is qualitatively different when the chromophore (coupled to the same baths) is excited by a pair of strong pulses ($\lambda_p = 1$), see Fig. 3. In contrast to Fig. 2, the signals $S(\tau)$ in panels (a) through (c) of Fig. 3 (left column) exhibit distinct vibrational beatings with the period τ_Ω. The explanation of this finding is as follows. In the weak-pulse limit, the signal is determined by the linear-response coherent contribution $S^{(c)}(\tau)$ (Eq. (4.3)). The population contribution $S^{(p)}(\tau)$ is proportional to λ_p^4 and is, therefore, much smaller than $S^{(c)}(\tau)$. For strong pulses, on the other hand, $S^{(c)}(\tau)$ and $S^{(p)}(\tau)$ contribute to $S(\tau)$ in a comparable manner. While $S^{(c)}(\tau)$ decays due to the bath-induced dephasing, $S^{(p)}(\tau)$ is unaffected by the dephasing. $S^{(p)}(\tau)$ mirrors vibrational wave-packet dynamics in the ground state and in the excited electronic state, which manifests itself through vibrational beatings in the overall $S(\tau)$. The oscillatory responses in Fig. 3 have nothing to do with electronic quantum coherences $\rho_{eg}(t)$ and can be considered as classical coherences.[63]

The Fourier transforms of the signals, $S(\omega)$, are shown in the right column of Fig. 3. For strong pulses, $S(\omega)$ cannot be interpreted as an absorption spectrum. Equation (3.3) tells us, however, that the double-slit signal represents the change of the energy of the primary system due to the interaction with pulse #2 (see, e.g., Ref. 27, Chapter 4), while the system dynamics is modified by pulse #1. It is, therefore, not surprising that $S(\omega)$ in panels (a) and (b) exhibits not only a pronounced absorption peak but also a negative contribution at $\omega \approx 44.5$, which corresponds to stimulated emission. The spectrum $S(\omega)$ in panel (c) appears almost structureless, although its counterpart $S(\tau)$ shows clear vibrational beatings. This example indicates that double-slit signals in the time domain may reveal finer details of the system dynamics than in the signals in the frequency domain.

Figure 4 shows double-slit signals in the case of strong system-bath coupling. Panels (a)-(c) of the figure correspond to those of Fig. 3, but the system-bath coupling is 10 times stronger ($\lambda_2 = 10$). Consideration of $S(\tau)$ (left column) reveals that the Markovian bath (panel (c)) effectively quenches the vibrational coherences. Nevertheless, strong pulses allow us to monitor the wave-packet dynamics of the system in highly dissipative and non-Markovian environments (panels (a) and (b)). In other words, the system dynamics induced by strong pulses competes successfully with bath-induced relaxations and dephasings, leading to the survival of vibrational beatings (see, e.g., discussions in Refs. 43 and 64–67). The Fourier transforms $S(\omega)$ are shown in the right panels of Fig. 4. $S(\omega)$ in panel (a) exhibits a peak at $\omega \approx 46.25$, corresponding to $\Omega/2$ (the central peak is at $\omega \approx 47.75$). A beating with this frequency can hardly be recognized in $S(\tau)$. When the width of the spectral function of the heat bath increases, $S(\omega)$ becomes featureless (panels (b) and (c)).

Figure 5 illustrates the effect of a low-temperature environment. The $S(\tau)$ in panels (a)-(c) of Fig. 5 correspond to those in Fig. 3, but the temperature is about an order of magnitude lower ($\beta\hbar\Omega_0 = 10.5$). Under these conditions, the chromophore initially resides in its vibrational ground state. As expected, the decay of $S(\tau)$ slows down at low temperature and becomes nonexponential. The weak-pulse signals exhibit

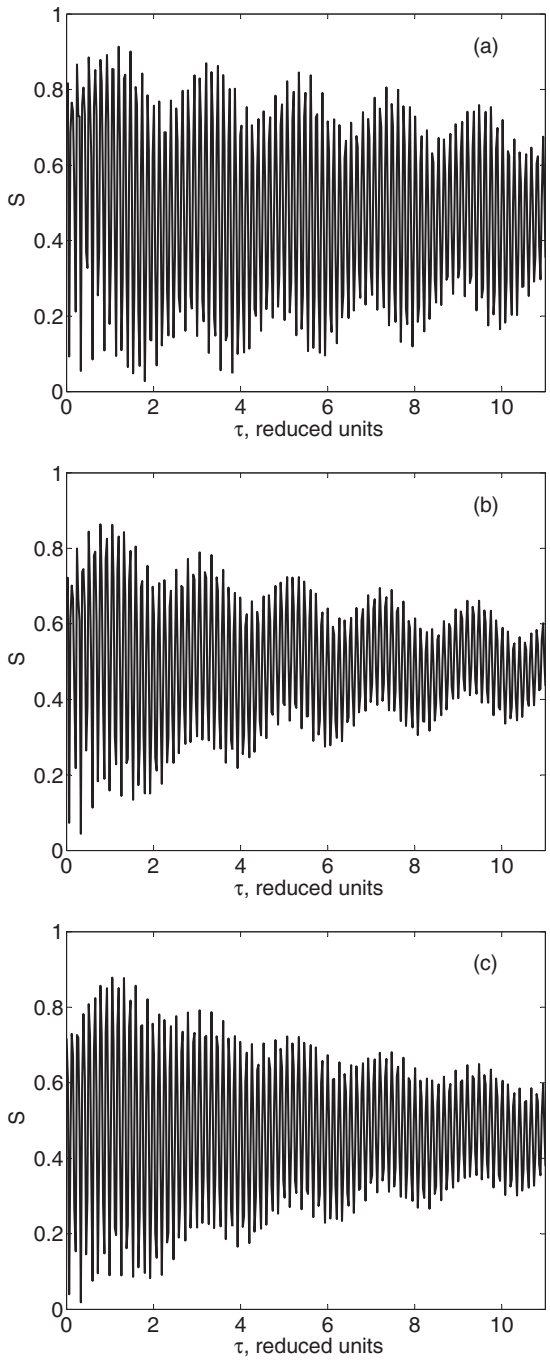

FIG. 5. Double-slit signal $S(\tau)$. The chromophore is excited by strong ($\lambda_p = 1$) and short ($\tau_p = 1.2$) pulses. The system-bath coupling is moderate ($\lambda_2 = 1$). The width of the spectral function of the bath is $\gamma = 0.1$ (panel (a)), $\gamma = 1$ (panel (b)), $\gamma = 10$ (panel (c)). The temperature is low ($\beta\hbar\Omega_0 = 10.5$).

a similar behavior, as follows from Eqs. (4.3) and (A13). Both electronic and vibrational beatings are pronounced in all panels. The Markovian bath (panel (c)) is most efficient in the quenching of vibrational beatings.

Figure 6 shows $S(\tau)$ calculated for the system and bath parameters of Fig. 3(c), but for pulses which are three times longer ($\tau_p = 3.6 > \tau_\Omega$). In this case, weak pulses cannot excite vibrational wave packets (not shown). Nevertheless, strong pulses with this duration can induce significant

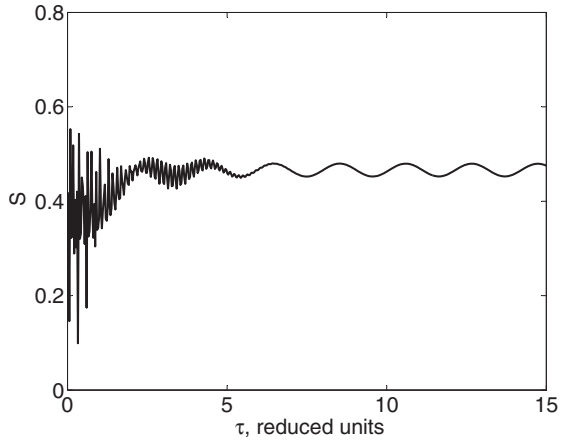

FIG. 6. Double-slit signal $S(\tau)$ generated with strong ($\lambda_p = 1$) and relatively long ($\tau_p = 3.6$) pulses for moderate system-bath coupling ($\lambda_2 = 1$) and a moderately non-Markovian bath ($\gamma = 1$) at ambient temperature ($\beta\hbar\Omega_0 = 0.5$).

vibrational wave-packet dynamics which can withstand the dephasing, resulting in clear vibrational beatings. Related phenomena have been studied and explained in Refs. 32 and 42.

Figure 7 illustrates that baths with different spectral functions can be very different with respect to the efficiency of quenching of the double-slit signal. The non-Markovian bath of Fig. 7 is equivalent to that of Fig. 4(a), but the coupling parameter λ_2 is 20 times larger. Despite the very strong system-bath coupling, the non-Markovian bath does not effectively quench the signal and vibrational beatings can still be observed. Similar findings have been reported for excitonic systems.[68]

Generally, non-Markovian baths are less efficient in quenching $S(\tau)$ than Markovian baths. However, the effect of a non-Markovian bath on $S(\tau)$ can be qualitatively modeled by a Markovian bath with a weaker coupling. It seems that the differences between Markovian and non-Markovian baths are more conspicuous in the frequency domain than in the time domain: Markovian baths yield narrower line shapes than non-Markovian baths (compare panels (a) and (c) in Figs. 2–4). The signal in the frequency domain is, however, proportional to the pulse spectrum $E(\omega)$, which complicates the extraction of the line shape (Lorenzian vs. Gaussian) of $S(\omega)$ if the spectral width of the pump pulses is smaller than the width of the absorption spectrum.

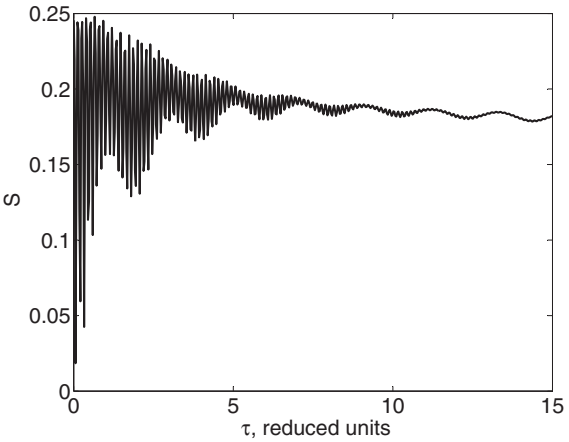

FIG. 7. Double-slit signal $S(\tau)$ generated by strong ($\lambda_p = 1$) and short ($\tau_p = 1.2$) pulses for very strong system-bath coupling ($\lambda_2 = 200$) and a non-Markovian bath ($\gamma = 0.1$) at ambient temperature ($\beta\hbar\Omega_0 = 0.5$).

VIII. CONCLUSIONS

We performed simulations of the prototypical double-slit experiment for a chromophore with a FC active mode in a dissipative environment. Our calculations treat the laser-matter coupling nonperturbatively, which allows us to simulate the dynamics of strongly driven material systems. Moreover, the system-bath coupling is treated numerically exactly with the HEOM method. Commonly used approximations, such as perturbation theory in the laser-matter coupling or Redfield theory, have been avoided. The simulations reported here are, therefore, of benchmark character and may be useful for the testing of the accuracy of more approximate, but computationally less demanding, methods.

We demonstrated that the double-slit signal generated with strong laser pulses can be considered as a superposition of N-wave mixing (N = 2, 4, 6...) signals. It can be split into population and coherence contributions, $S(\tau) = S^{(p)}(\tau) + S^{(c)}(\tau)$. The former provides information on the dynamics of vibrational wave packets in the ground state and the excited electronic state of the chromophore, while the latter monitors the time evolution of the electronic coherences of the chromophore density matrix.

We studied how heat baths with different coupling strengths and memories affect the double-slit signal. Our main finding can be summarized as follows: When the bath-induced dephasing is effective, the strong-pulse double-slit experiment yields more information on the dynamics of the material system than the weak-pulse double-slit experiment.

The coherent responses triggered by intensive phase-locked pulses are not specific for the particular model system considered here, but are generic for photochemically nonreactive polyatomic molecules in solution. For example, double-slit strong-field spectroscopy may be employed to unravel the condensed-phase dynamics of molecular chromophores possessing weak electronic transitions (see, e.g., Ref. 69) or weakly FC-active vibrational modes in the presence of strong electronic dephasing. Probing the dynamics of high-lying electronic states of molecular systems with intense pulses may become another promising research topic (cf. Ref. 32). Strong-pulse double-slit experiments on systems exhibiting photochemical reactions (e.g., photoinduced electron-transfer or proton-transfer reactions) or on multi-chromophoric systems should be considered in the future.

ACKNOWLEDGMENTS

M.F.G. and W.D. acknowledge the support from the Deutsche Forschungsgemeinschaft (DFG) through a research grant and the DFG-Cluster of Excellence "Munich-Centre for Advanced Photonics" (http://www.munich-photonics.de). Y.T. is grateful for the hospitality of Wolfgang Domcke and his group members at the Technical University of Munich.

Y.T. acknowledges support from the Humboldt Foundation and a Grant-in-Aid for Scientific Research (B2235006) from the Japan Society for the Promotion of Science.

APPENDIX A: EVALUATION OF THE LINESHAPE FUNCTIONS

Consider the Hamiltonian defined by Eqs. (2.1), (2.2), and (2.4). The corresponding lineshape function $g(t)$ consists of two contributions due to the FC-active mode ($g_1(t)$) and the bath ($g_2(t)$):

$$g(t) = g_1(t) + g_2(t). \tag{A1}$$

Both of them can be cast into the form

$$g_i(t) = \int_0^t d\tau \int_0^\tau d\tau' \left[C_i(\tau') - \frac{i\hbar}{2}\chi_i(\tau') \right] \tag{A2}$$

($i = 1, 2$), where $\chi_i(t) = -\chi_i(-t)$ and $C_i(t) = C_i(-t)$ are the anti-symmetric and symmetric coordinate correlation functions, respectively.

For the FC-active vibrational mode,[27]

$$\chi_1(t) = i \langle [Q(t), Q] \rangle / \hbar, \tag{A3}$$

$$C_1(t) = \langle \{Q(t), Q\} \rangle / 2, \tag{A4}$$

and

$$g_1(t) = \lambda_1 \left\{ \coth\left(\frac{\hbar\Omega\beta}{2}\right)(1 - \cos(\Omega t)) + i(\sin(\Omega t) - \Omega t) \right\}, \tag{A5}$$

$$\lambda_1 = \Delta^2 \Omega / 2.$$

For $g_2(t)$, we define the collective bath coordinate as

$$q = \sum\nolimits_\alpha q_\alpha. \tag{A6}$$

The anti-symmetric correlation function is responsible for bath-induced fluctuations,

$$\chi_2(t) = i \langle [q(t), q] \rangle / \hbar, \tag{A7}$$

while the symmetric correlation function is responsible for dissipation,

$$C_2(t) = \langle \{q(t), q\} \rangle / 2. \tag{A8}$$

$\chi_2(t)$ and $C_2(t)$ are related by the fluctuation-dissipation theorem (see, e.g., Refs. 26 and 27). They can be expressed through the bath spectral distribution (2.5) as follows:

$$\chi_2(t) = \frac{2}{\hbar} \int_0^\infty d\omega J(\omega) \sin(\omega t), \tag{A9}$$

$$C_2(t) = \int_0^\infty d\omega J(\omega) \cos(\omega t) \coth(\beta\hbar\omega/2). \tag{A10}$$

For the Drude spectral distribution (6.2), $\chi_2(t)$ and $C_2(t)$ can be evaluated analytically:[26,27]

$$\chi_2(t) = \frac{\lambda_2 \gamma}{\hbar} e^{-\gamma t}, \tag{A11}$$

$$C_2(t) = \lambda_2 \gamma \left\{ \frac{1}{2} \cot\left(\frac{\beta\hbar\gamma}{2}\right) e^{-\gamma t} + \frac{2}{\beta\hbar} \sum_{k=1}^{\infty} \frac{\nu_k}{\nu_k^2 - \gamma^2} e^{-\nu_k t} \right\}. \tag{A12}$$

Here, $\beta \equiv 1/(k_B T_{eq})$ is the inverse temperature and $\nu_k = 2\pi k/(\hbar\beta)$ are the Matsubara frequencies. Finally, the bath lineshape function is given by

$$g_2(t) = \frac{\lambda_2}{2\gamma} \{e^{-\gamma t} + \gamma t - 1\} \left(\cot\left(\frac{\hbar\gamma\beta}{2}\right) - i \right) + \frac{2\lambda_2\gamma}{\hbar\beta} \sum_{k=1}^{\infty} \frac{e^{-\nu_k t} + \nu_k t - 1}{\nu_k(\nu_k^2 - \gamma^2)}. \tag{A13}$$

APPENDIX B: STRONG-PULSE DOORWAY-WINDOW APPROXIMATION

To cast the double-slit signal into DW form, we follow the derivations of Refs. 32 and 40. Assuming that the pulses #1 and #2 are temporally well separated (that is, the time interval between the pulses, τ, is much longer than the pulse duration τ_p), we can write

$$S(\tau) \equiv \langle W G(\tau) D \rangle, \tag{B1}$$

where

$$D = G_1(\delta_1, -\delta_1)\rho_0 \tag{B2}$$

is the doorway (D) operator and

$$W = \int_{-\delta_2}^{\delta_2} dt E^*(t) X^\dagger G_2(t, -\delta_2) \tag{B3}$$

is the window (W) operator. The $G_a(t, t')$ are the evolution operators governing the driven dynamics of the FC-active mode induced by the pulse #a, $G(t - t')$ is the stationary field-free evolution operator, and ρ_0 is the initial system distribution. The arrival times of pulses #1 and #2 have been set to zero ($\tau_a = 0$). $[-\delta_a, \delta_a]$ are the time intervals outside of which the action of pulse #a can be neglected.

In general (e.g., for pump-probe spectroscopy) Eq. (B1) is not the final expression for the optical signal: One has to extract the components of D and W which obey the appropriate phase matching condition.[32,40] In the "double slit" experiment, on the other hand, there is no external phase selection. Nonetheless, it is instructive to determine the phase dependence of the signal explicitly. This can immediately be done by using Eqs. (A9) and (A10) of Ref. 40:

$$D_{gg} \sim 1, D_{ee} \sim 1, D_{eg} \sim e^{i\phi_1}, D_{ge} \sim e^{-i\phi_1}, \tag{B4}$$

$$W_{gg} \sim 1, W_{ee} \sim 1, W_{eg} \sim e^{i\phi_2}, W_{ge} \sim e^{-i\phi_2}. \tag{B5}$$

Here, $D_{kn} \equiv \langle k|D|n\rangle$, $W_{kn} \equiv \langle k|W|n\rangle$, $k, n = e, g$. Inserting Eqs. (B4) and (B5) into Eq. (B1), we arrive at formulas (5.2) and (5.3).

[1] N. F. Scherer, R. J. Carlson, A. Matro, Mei Du, A. J. Ruggiero, V. Romero-Rochin, J. A. Cina, G. R. Fleming, and S. A. Rice, J. Chem. Phys. **95**, 1487 (1991).
[2] N. F. Scherer, A. Matro, L. D. Ziegler, M. Du, R. J. Carlson, J. A. Cina, and G. R. Fleming, J. Chem. Phys. **96**, 4180 (1992).

[3] K. Ohmori, Annu. Rev. Phys. Chem. **60**, 487 (2009).
[4] J. A. Cina, Annu. Rev. Phys. Chem. **59**, 319 (2008).
[5] M. Fushitani, Annu. Rep. Prog. Chem., Sect. C: Phys. Chem. **104**, 272 (2008).
[6] V. Blanchet, M. A. Bouchène, and B. Girard, J. Chem. Phys. **108**, 4862 (1998).
[7] C. Warmuth, A. Tortschanoff, F. Milota, M. Shapiro, Y. Prior, I. S. Averbukh, W. Schleich, W. Jakubetz, and H. F. Kauffmann, J. Chem. Phys. **112**, 5060 (2000).
[8] M. Fushitani, M. Bargheer, M. Gühr, and N. Schwenter, Phys. Chem. Chem. Phys. **7**, 3143 (2005).
[9] N. F. Ramsey, Appl. Phys. B **60**, 85 (1995).
[10] M. M. Salour, Rev. Mod. Phys. **50**, 667 (1978).
[11] S. Witte, R. T. Zinkstok, W. Ubachs, W. Hogervorst, and K. S. E. Eikema, Science **307**, 400 (2005).
[12] R. Bavli, V. Engel, and H. Metiu, J. Chem. Phys. **96**, 2600 (1992).
[13] G. M. Lankhuijzen and L. D. Noordam, Phys. Rev. A **52**, 2016 (1995).
[14] R. R. Jones, D. W. Schumacher, T. F. Gallagher, and P. B. Bucksbaum, J. Phys. B **28**, L405 (1995).
[15] R. R. Jones, C. S. Raman, D. W. Schumacher, and P. B. Bucksbaum, Phys. Rev. Lett. **71**, 2575 (1993).
[16] C. Nicole, M. A. Bouchène, S. Zamith, N. Melikechi, and B. Girard, Phys. Rev. A **60**, R1755 (1999).
[17] M. Wollenhaupt and T. Baumert, Faraday Discuss. **153**, 9 (2011).
[18] R. Hildner, D. Brinks, F. D. Stefani, and N. F. van Hulst, Phys. Chem. Chem. Phys. **13**, 1888 (2011).
[19] R. Hildner, D. Brinks, J. B. Nieder, R. J. Cogdell, and N. F. van Hulst, Science **340**, 1448 (2013).
[20] D. Brinks, R. Hildner, F. D. Stefani, and N. F. van Hulst, Faraday Discuss. **153**, 51 (2011).
[21] W. Kuehn, K. Reimann, M. Woerner, and T. Elsaesser, J. Chem. Phys. **130**, 164503 (2009).
[22] W. Kuehn, K. Reimann, M. Woerner, T. Elsaesser, and R. Hey, J. Phys. Chem. B **115**, 5448 (2011).
[23] Y. Tanimura and R. Kubo, J. Phys. Soc. Jpn. **58**, 101 (1989)
[24] Y. Tanimura and P. G. Wolynes, Phys. Rev. A **43**, 4131 (1991).
[25] A. Ishizaki and Y. Tanimura, J. Phys. Soc. Jpn. **74**, 3131 (2005).
[26] Y. Tanimura, J. Phys. Soc. Jpn. **75**, 082001 (2006).
[27] S. Mukamel, *Principles of Nonlinear Optical Spectroscopy* (Oxford University Press, New York, 1995).
[28] L. Allen and J. H. Eberly, *Optical Resonance and Two-Level Atoms* (Dover, New York, 1987).
[29] M. Tanaka and Y. Tanimura, J. Phys. Soc. Jpn. **78**, 073802 (2009).
[30] M. Tanaka and Y. Tanimura, J. Chem. Phys. **132**, 214502 (2010).
[31] Y. Tanimura, J. Chem. Phys. **137**, 22A550 (2012).
[32] M. F. Gelin, D. Egorova, and W. Domcke, Phys. Chem. Chem. Phys. **15**, 8119 (2013).
[33] A. Kaiser and V. May, Chem. Phys. **320**, 95 (2006).
[34] Y. Tanimura and S. Mukamel, Phys. Rev. E **47**, 118 (1993).
[35] Y. Tanimura and K. Okumura, J. Chem. Phys. **106**, 2078 (1997).
[36] M. Cho, N. F. Scherer, G. R. Fleming, and S. Mukamel, J. Chem. Phys. **96**, 5618 (1992).
[37] M. F. Gelin, C. Riehn, M. Kunitski, and B. Brutschy, J. Chem. Phys. **132**, 134301 (2010).
[38] Y. J. Yan, L. E. Fried, and S. Mukamel, J. Phys. Chem. **93**, 8149 (1989).
[39] L. E. Fried and S. Mukamel, J. Chem. Phys. **93**, 3063 (1990).
[40] M. F. Gelin, D. Egorova and W. Domcke, J. Phys. Chem. B **115**, 5648 (2011).
[41] Y. Tanimura and S. Mukamel, J. Phys. Chem. **97**, 12596 (1993).
[42] M. F. Gelin, D. Egorova, and W. Domcke, J. Phys. Chem. Lett. **2**, 114 (2011).
[43] Y. Tanimura and Y. Maruyama, J. Chem. Phys. **107**, 1779 (1997).
[44] A. Ishizaki and Y. Tanimura, J. Phys. Chem. A **111**, 9269 (2007).
[45] A. Sakurai and Y. Tanimura, J. Phys. Chem. A **115**, 4009 (2011).
[46] F. Jiang, J. Jin, S. Wang, and Y.-J. Yan, Phys. Rev. B **85**, 245427 (2012).
[47] A. G. Dijkstra and Y. Tanimura, Phys. Rev. Lett. **104**, 250401 (2010).
[48] A. G. Dijkstra and Y. Tanimura, J. Phys. Soc. Jpn. **81**, 063301 (2012).
[49] X. Yin, J. Ma, X. Wang, and F. Nori, Phys. Rev. A **86**, 012308 (2012).
[50] A. Ishizaki and G. R. Fleming, Proc. Natl. Acad. Sci. U.S.A. **106**, 17255 (2009).
[51] L. Chen, R. Zheng, Y. Jing, and Q. Shi, J. Chem. Phys. **134**, 194508 (2011).
[52] C. Kreisbeck and T. Kramer, J. Phys. Chem. Lett. **3**, 2828 (2012).
[53] J. Strümpfer and K. Schulten, J. Chem. Phys. **137**, 065101 (2012).
[54] A. G. Dijkstra and Y. Tanimura, New J. Phys. **12**, 055005 (2010).
[55] R.-X. Xu, Y. Chen, P. Cui, H. W. Ke, and Y.-J. Yan, J. Phys. Chem. A **111**, 9618 (2007).
[56] Y. Tanimura and S. Mukamel, J. Phys. Soc. Jpn. **63**, 66 (1994).
[57] Q. Shi, L. P. Chen, G. J. Nan, R. X. Xu, and Y.-J. Yan, J. Chem. Phys. **130**, 084105 (2009).
[58] J. Hu, R. X. Xu, and Y.-J. Yan, J. Chem. Phys. **133**, 101106 (2010).
[59] B. L. Tian, J. J. Ding, R. X. Xu, and Y.-J. Yan, J. Chem. Phys. **133**, 114112 (2010).
[60] C. Kreisbeck, T. Kramer, M. Rodriguez, and B. Hein, J. Chem. Theor. Comput. **7**, 2166 (2011).
[61] J. Zhu, S. Kais, P. Rebentrost, and A. Aspuru-Guzik, J. Phys. Chem. B **115**, 1531 (2011).
[62] J. Strümpfer and K. Schulten, J. Chem. Theor. Comput. **8**, 2808 (2012).
[63] W. H. Miller, J. Chem. Phys. **136**, 210901 (2012).
[64] V. I. Prokhorenko, A. Halpin, P. J. M. Johnson, R. J. D. Miller, and L. S. Brown, J. Chem. Phys. **134**, 085105 (2011).
[65] D. Egorova, M. F. Gelin, M. Thoss, H. Wang, and W. Domcke, J. Chem. Phys. **129**, 214303 (2008).
[66] M. F. Gelin, D. Egorova, and W. Domcke, J. Chem. Phys. **131**, 124505 (2009).
[67] U. Banin, A. Bartana, S. Ruhman, and R. Kosloff, J. Chem. Phys. **101**, 8461 (1994).
[68] A. Ishizaki and G. R. Fleming, J. Chem. Phys. **130**, 234111 (2009).
[69] M. F. Gelin, A. K. Belyaev, and W. Domcke, Phys. Rev. A **87**, 063416 (2013).